This article has been accepted for publication in a future issue of this journal, but has not been fully edited. Content may change prior to final publication. Citation information: DOI 10.1109/JRFID.2020.2998082, IEEE Journal of Radio Frequency Identification

Epidermal Backscattering Antennas in the 5G Framework: Performance and Perspectives

Francesco Amato, *Member, IEEE,* Cecilia Occhiuzzi, *Member, IEEE,* and Gaetano Marrocco, *Member, IEEE*

***Abstract*—Epidermal RFIDs, if integrated within the next-generation (5G) wireless architecture, would enable low-cost healthcare applications for remote monitoring of patients, real-time telesurgery, and augmented sensing abilities. This paper explores, through simulations and preliminary experiments, epidermal 5G-RFIDs operating both at microwave and mmWave frequencies. In particular, it identifies the maximum gains of epidermal antennas at their optimal sizes, the achievable read ranges of passive 5G-RFID links, and their possible data-rates. Moreover, it demonstrates the compliance with electromagnetic exposure regulations and explores the benefits of epidermal arrays. Loop transponders at microwave frequencies (3.6 GHz) could provide the same read distance (one meter) of their UHF counterparts while having a smaller footprint (17 x 17 mm^2) and reaching a theoretical data-rate as high as 0.5 Gbps. At 28 GHz and 60 GHz, instead, arrays could be used to both achieve comparable performances and enable beamsteering.**

***Index Terms*—5G, RFID, backscattering, epidermal sensors, Body sensor Networks, mmWave.**

I. Introduction

Epidermal Electronics [1] is currently pushing personal wireless devices from being simply worn on clothes to be directly attached on the human skin. Indeed, new wireless flexible and stretchable sensors have been recently proposed (up to the pioneering neonatal intensive care [2]) for collecting both physical and chemical parameters directly from the epidermis (*e.g.:* temperature [3], breath [4], sweat [5], and pH [6]). The core of these devices are membrane-like antennas operating in HF (13.56 MHz) and UHF (860-960 MHz) bands coupled with electrochemical (bio)sensors and transponders [7]. Low-cost, comfortable and thin configurations suitable for the skin (Fig. 1) are only possible with battery-less architectures based on Radiofrequency Identification (RFID). UHF-RFID readers can currently interrogate *passive epidermal sensors* up to 1-1.5 meters [8] and collect biophysical parameters through modulated backscattering communication.

One bottleneck of passive *epidermal* electronics is the short communication range. Losses due to the human body degrade the radiation efficiency of epidermal antennas thus reducing the reading ranges. Conventional mitigation remedies for passive *wearable* antennas cannot be applied to *epidermal* ones since they aim at reducing the electromagnetic interaction with the body through either thick/rigid insulating dielectrics, or grounded layouts (like patch antennas), or meta-material layers [9]. These decoupling layers yield bulk and un-stretchable configurations that are neither breathable nor suitable to measure epidermal parameters. The narrow bandwidths at HF and UHF frequencies, moreover, prevent the simultaneous readout of either multiple epidermal signals like ECG, EEG, and EMG, or the slower variable temperature and sweat when a user is walking or running across a reading gate (*e.g.:* for sport events, for wellness applications, and for critical scenarios). Finally, the need of dedicated readers to interrogate RFID sensors impacts their use and diffusion.

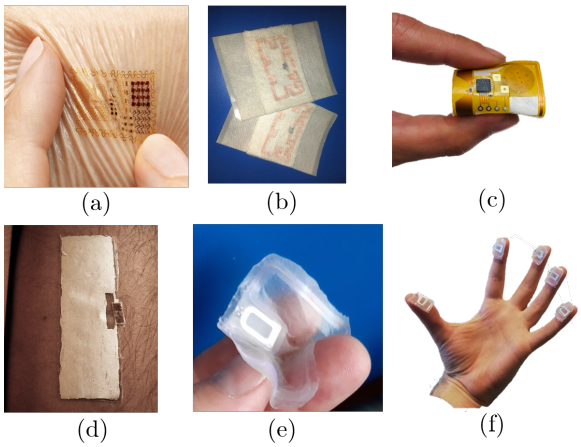

Fig. 1: Examples of state-of-the-art Epidermal battery-less RFID transponders in HF and UHF bands. a) Tattoo-like coil [1]; b) meandered-line loops within plasters [10]; c) general purpose flexible board for external sensor interconnection [8]; d) conductive ink tattoo antenna [11]; e) stretchable epidermal tag for temperature measurement [12]; and f) fingertip antennas for Sensing UltrAbility [13].

In the next years a convergence of Epidermal Electronics with the forthcoming Fifth Generation (5G) wireless communication systems is expected. 5G pledges to provide a massive amount of bandwidth, low latency (down to 1 ms), and multigigabit-per-second (Gbps) data rates through both the sub-6 GHz bands and the mmWave frequency spectrum [14]. The capability to manage huge amount of data will encourage the deployment of countless epidermal sensors for high-speed Personal Area Networks (PAN) streaming at bit-rates going beyond the few tens of Hertz of today. It will be possible to download data from multiple sensors either deployed onto a single user, to collect detailed maps of biophysical processes, or to simultaneously monitor multiple people in a specific area. The low latency will enable epidermal digital twins to monitor

F. Amato, C. Occhiuzzi, and G. Marrocco are with the Pervasive Electromagnetic Lab, Department of Civil and Computer Science Engineering, University of Roma Tor Vergata, 00133 Rome, Italy (e-mail: f.amato@ieee.org, {francesco.amato, gaetano.marrocco, cecilia.occhiuzzi}@uniroma2.it). Work supported by Lazio Innova within "Programma Gruppi di Ricerca - SECOND SKIN", grant n. 85-2017-14774 and by the University of Rome Tor Vergata within "Beyond Borders - Epidermal Sensor Networks for Emerging 5G systems", grant n. E84I19002410005.

2469-7281 (c) 2020 IEEE. Personal use is permitted, but republication/redistribution requires IEEE permission. See http://www.ieee.org/publications_standards/publications/rights/index.html for more information.
Authorized licensed use limited to: Universita degli Studi di Roma Tor Vergata. Downloaded on June 04,2020 at 11:13:04 UTC from IEEE Xplore. Restrictions apply.

This article has been accepted for publication in a future issue of this journal, but has not been fully edited. Content may change prior to final publication. Citation information: DOI 10.1109/JRFID.2020.2998082, IEEE Journal of Radio Frequency Identification

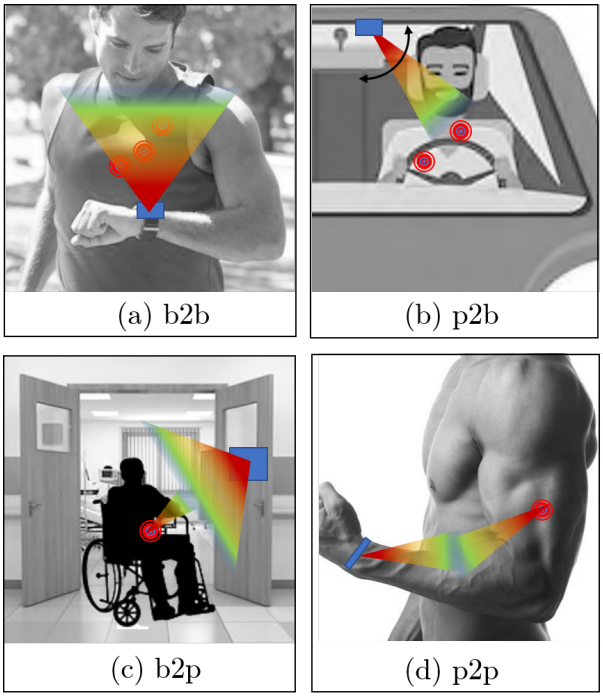

Fig. 2: Possible scenarios of epidermal sensor networks at 5G frequencies: a) smart-watch (or smartphone) retrieving multiple bio-physical data from the user; b) smart car monitoring the stress level of a driver to prevent accidents; c) smart house checking, in real-time, the health status of elders; and d) high-accuracy real-time tracking of muscle contractions for precise sport training and rehabilitation support.

interactions and tactile sensing during remote medical diagnosis. Moreover, thanks to the interoperability of 5G systems, an epidermal sensor used as a *smart electronic plaster* will be able to communicate with other network devices such as implanted sensors, wearable gateways (smartphone, smartwatch or smart ear-buds), and external base stations for in-/on-/off-body communications (Fig. 2). The expected millimeter-scale of 5G-epidermal devices will, moreover, allow epidermal-arrays to shape the radiating beam towards specific directions.

The possibility to exploit mmWave frequency bands for body area networks have already gathered great interest mainly concerning *wearable antennas* [15] and the corresponding communication links [16]. Examples of 60 GHz wearable antennas can be found in [15], [16], while the advantages of small arrays have been preliminary explored in [17]. The effects of mmWave radiations on heating and penetration of the human body were theoretically discussed in [18]. Finally, mmWave Identifications (MMID) at 60 GHz, by using non-epidermal oriented passive tags responding through modulated backscattering, demonstrated a theoretical link range up to 30 cm in free-space by assuming the typical sensitivity of UHF ICs and readers [19].

Backscattering through *epidermal antennas* at 5G frequencies has not been investigated yet. Nonetheless, the feasibility itself of a battery-less backscattering-based link is still in question due to both the higher human body losses at these frequencies and the increased free-space path-loss.

TABLE I: 5G Frequency Bands and Services

Bands		Frequency	Services
UHF		700 MHz	Wide-rural area & indoor mobile
μWaves	**S- & C-bands**	3.3 - 4.2 GHz 4.4 - 5.0 GHz (3.6 GHz in EU [22])	Outdoor Mobile
	K- & Ka bands	24 - 28 GHz & 37 - 40 GHz	Mobile & IoT
mmWaves	**V-band**	60 GHz	Indoor WiFi & IoT

Starting from the preliminary results in [20] and from the state-of-the-art in epidermal UHF tags, this paper derives, for the first time, the upper-bound performances of 5G-RFID epidermal antennas in terms of maximum gains and optimal frequencies (Sec. III) as well as achievable read ranges and possible data-rates (Sec. IV). Optimal sizes are identified and the use of multiple antennas to form epidermal beam-steering arrays are explored while their compliance with the regulations on electromagnetic exposure is verified (Sec. V). The theory is supported by numerical simulations and by preliminary experimental tests on living tissues.

II. 5G Spectrum and Link Equations

A. 5G Frequencies

In August 2017, the 3GPP[1] [21] consortium and, consequently, governments and operators from Europe, the US, Japan, Canada and China [22][23] agreed on the 5G New Radio (NR) frequency spectrum as summarized in Tab I; it includes the sub-6 GHz bands, *i.e.*: UHF, S-, and C-bands; and the above-6 GHz bands, *i.e.*: K-, Ka-, and V-bands. Presently, 5G mmWave cellular bands are primarily centered in two regions (24 GHz to 28 GHz, and 37 GHz to 40 GHz), while the 60 GHz band is available worldwide for unlicensed operation to extend the capabilities of indoor WiFi systems into mmWave frequencies.

B. Communication Links for Epidermal Devices

A reader and a tag can communicate through four types of wireless links depending on the directivity of the involved antennas. In case of wireless sensors located on the body (either wearable or epidermal), it is possible to identifies the four scenarios shown in Fig. 2:

b2b - broadcast-to-broadcast links: both the reader and the tag are equipped with omnidirectional antennas (Fig. 2a). This link allows short-distance on-body communications, with many epidermal sensors displaced across the body and not too far from the transmitting hub;

p2b - point-to-broadcast links: a directive (either on-body or external) reader can interrogate only a sub-set of on-body sensors mounting omnidirectional tag antennas (Fig. 2b);

b2p - broadcast-to-point links: an omnidirectional reader reaches one (or more) body sensor tags equipped with directional antennas for real-time high data-rate communications (Fig. 2c);

p2p - point-to-point links: both the reader and tags are equipped with directive antennas to either boost the read

[1]Third Generation Partnership Project

2469-7281 (c) 2020 IEEE. Personal use is permitted, but republication/redistribution requires IEEE permission. See http://www.ieee.org/publications_standards/publications/rights/index.html for more information.
Authorized licensed use limited to: Universita degli Studi di Roma Tor Vergata. Downloaded on June 04,2020 at 11:13:04 UTC from IEEE Xplore. Restrictions apply.

This article has been accepted for publication in a future issue of this journal, but has not been fully edited. Content may change prior to final publication. Citation information: DOI 10.1109/JRFID.2020.2998082, IEEE Journal of Radio Frequency Identification

distances, or enable wireless transfer of power [24], or increase localization accuracy (Fig. 2d).

C. Communications and Antenna Sizes

Since RFID-based communication links require the harvesting of power for turning on the circuitry of the tags, their limited read distance affects the possible applications. For the next discussions, the gain G of an epidermal antenna is expressed in terms of the effective aperture area A_e:

$$A_e = \eta_A A_p = \frac{c^2}{4\pi f^2} G, \tag{1}$$

where A_p is the physical area of the antenna, and $\eta_A \leq 1$ is the aperture efficiency. Therefore, both the free-space Friis [25] and Radar equations for the forward and the backward links, respectively, can be written as:

$$P_{R\rightarrow T} = P_{in} A_{e,R} A_{e,T} \eta_p \tau_R \tau_T \left(\frac{f}{cr}\right)^2, \tag{2}$$

$$P_{R\leftarrow T} = P_{in} A_{e,R}^2 A_{e,T}^2 \eta_p \tau_R M \left(\frac{f}{cr}\right)^4, \tag{3}$$

where η_p is the polarization mismatch between the two antennas; τ_R and τ_T are the power transfer coefficients at the ports of the reader and transponder, respectively[2] located at distance r from each-others; $A_{e,R}$ and $A_{e,T}$ are the antenna effective apertures of the reader and transponder, respectively, with gains G_R, and G_T; *M* is the modulation index; and c is the speed of light.

If p_t and p_r are the transponder and reader sensitivities, respectively, the maximum read distance is the minimum between the maximum forward link range, r_F^{max} ($P_{R\rightarrow T} = p_t$), and the maximum backward link range, r_B^{max} ($P_{R\leftarrow T} = p_r$):

$$r^{max} = min \begin{cases} r_F^{max} = \sqrt{\frac{P_{in} A_{e,R} A_{e,T}}{p_t}} \frac{f}{c} \\ r_B^{max} = \sqrt[4]{\frac{P_{in} A_{e,R}^2 A_{e,T}^2 M}{p_r}} \frac{f}{c} \end{cases} \tag{4}$$

Since 5G-oriented electronics for backscattering radios are not yet available, it will be hereafter assumed that the sensitivities of current state-of-the-art UHF-RFID components ($p_t = -15$ dBm [27] and $p_r = -82$ dBm [28], [29], [30]) could be achieved with 5G frequencies as well. Due to the low radiation efficiency of epidermal antennas, the communication bottleneck remains the forward link for passive RFID tags [19] hence, only this link will be hereafter investigated.

For a fixed value of input power and transponder sensitivity, the maximum read range changes with f so that $r^{max} \propto A_e^{\frac{1}{2}} f \propto G^{\frac{1}{2}}/f$. Thus, when the frequency increases by moving from UHF to mmWaves, and the radiation gains remain the same (*i.e.:* the effective apertures shrink), then the read distance decreases as $1/f$, with huge impact on the feasibility of a 5G backscattering link. Instead, if at least one of the effective apertures remains constant despite the higher frequency (*i.e.:* the radiation gains increase), then the same communication performance can be achieved at both UHF, microwave and mmW bands. For this purpose, the gain of at least one of the two antennas has to increase with frequency according to a quadratic law:

$$G(f) = af^2, \tag{5}$$

with a being constant. Furthermore, even better performances than UHF could be achieved at 5G frequencies provided that the gains of both the reader and the tag obey to (5).

The question is how to improve the gain of an epidermal antenna when operating at higher frequencies. The problem is not trivial because of the direct contact with the human body and, hence, the limited possibilities in designing high directive antennas. For the sake of simplicity, only the *b2b* link will be here analyzed because power emission regulations limit the maximum gain of a reader antenna, while no constraints are expected for the passive transponder beside the fabrication issues. Therefore, the reader gain G_R is hereafter assumed constant with the frequency and considerations will be made only on the transponder side. The benchmark will be the read range r_{UHF}^{max} of an optimal epidermal UHF RFID tag of effective area A_{UHF}^{max}.

III. Optimal Size of Epidermal Antennas at 5G Frequencies

As recently demonstrated in [31], the upper-bound performance of UHF epidermal antennas is rather independent on their specific layout (dipole, loop, slot), but it is affected by a trade-off between the radiation resistance and the loss resistance of the tissues both related to the antenna footprint. Typical radiation gains fall in the range $[-18, -12]$ dBi depending on the skin-to-antenna distance and on the material of the interposed substrate. Typical substrates must be flexible, possibly stretchable, and bio-compatible. They can either be very thin (below 1 mm), and with low permittivity ($\epsilon_r \sim 1$), like the highly porous and fibrous Polycaprolactone membrane, and the Ethylene Propylene Diene Monomer (EPDM) foam, or thicker and denser, like the Bio-silicone ($\epsilon_r \sim 2.5$), and the polyvinyl alcohol Xyloglucan-based hydrogels ($\epsilon_r \sim 30$).

Optimal performance analysis of epidermal antennas is here explored through numerical simulations on body models at some representative 5G frequencies, $f_{5G} = \{3.6, 28, 60\}$ GHz. Due to the broad 5G frequency spectrum, the choice of body models and constitutive parameters deserve some preliminary considerations.

A. Human Body Model at 5G Frequencies

As demonstrated in [18], more than 90% of the transmitted electromagnetic power is absorbed at mmWave bands within the epidermis (60 - 100 μm) and dermis layers (1.2 - 2.8 mm), while much less power penetrates further into deeper

[2]Since the aim of this work is to derive the upper-bound performances of the 5G-RFID link, it is assumed that $\eta_p = 1$, *i.e.* co-polarized reader and tag antennas and, for the same reason, both antennas are assumed perfectly matched so that $\tau_R = \tau_T = 1$. Antenna matching can be achieved through T-match, Gamma-match, or loop-match [26].

2469-7281 (c) 2020 IEEE. Personal use is permitted, but republication/redistribution requires IEEE permission. See http://www.ieee.org/publications_standards/publications/rights/index.html for more information.
Authorized licensed use limited to: Universita degli Studi di Roma Tor Vergata. Downloaded on June 04,2020 at 11:13:04 UTC from IEEE Xplore. Restrictions apply.

This article has been accepted for publication in a future issue of this journal, but has not been fully edited. Content may change prior to final publication. Citation information: DOI 10.1109/JRFID.2020.2998082, IEEE Journal of Radio Frequency Identification

tissues. Instead, the penetration of microwaves at sub-6 GHz bands exceeds the typical skin thickness and reaches the inner tissues of fat and muscles.

The well-established model of Gabriel & Gabriel [32] is the recognized standard for body tissues at both UHF and microwave frequencies. Recently, Chahat *et al.* [33] developed a single-term Cole-Cole model for the skin that is based on direct measurements on wrist, forearm and palm at frequencies ranging between 10 GHz and 60 GHz. The two models are compared in Fig. 3. At the highlighted 5G frequency bands, the conductivity σ of the tissues rises of more than an order of magnitude w.r.t. UHF, while the permittivity ϵ_r decreases of a comparable amount. Relaxation takes place at around 10 GHz and, above these values, some differences between the Chahat and the Gabriel models are visible for the electromagnetic parameters of the skin.

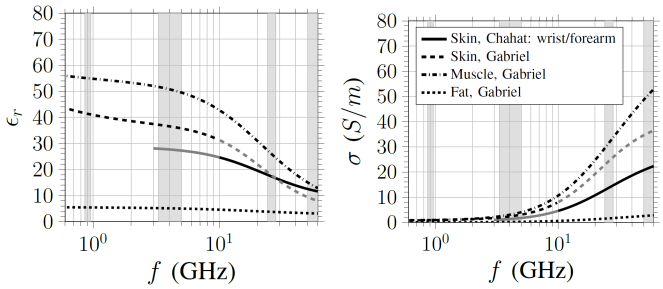

Fig. 3: (a) Relative permittivities ϵ_r and (b) conductivities σ for muscle, fat and skin according to Gabriel [32] and Chahat [33]. Gray lines indicate extrapolated parameters. The UHF and 5G frequencies bands of interest are highlighted in gray.

Fig. 4 summarizes the numerical analyses performed with CST Microwave Studio© on a half-wavelength dipole (length $L = \frac{c}{2f_{5G}}$) suspended at 0.25 mm from flat layered models of the human body. The 3-layer model returns same gain values regardless of the adopted electromagnetic parameters in the entire 3.6-60 GHz band. The 1-layer model, instead, is adequate only for frequencies above 20 GHz. The gain drops at around 10 GHz where relaxation takes place. Accordingly, in the following numerical simulations, the 3-layer model will be used at 3.6 GHz and the 1-layer model will be adopted at both 28 GHz and 60 GHz with the electromagnetic parameters summarized in Tab. II.

TABLE II: Selected Permittivity and Conductivity Values for the Human Body Model

Layers		Freq. (GHz)		
		3.6 Gabriel [32]	28 Chahat [33]	60 Chahat [33]
Skin	ϵ_r	36.92	16.65	11.61
1* or 2† mm	σ (S/m)	2.08	14.65	22.32
Fat	ϵ_r	5.16	-	-
3 mm	σ (S/m)	0.16		
Muscle	ϵ_r	51.32		
31 mm	σ (S/m)	2.65		

*at 3.6 GHz; †at 28 and 60 GHz.

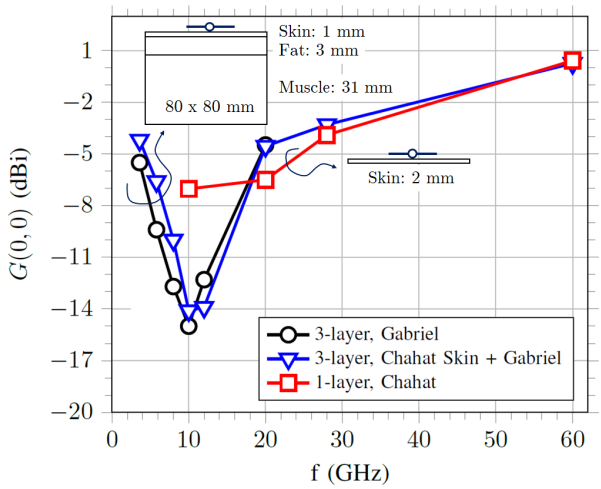

Fig. 4: Broadside gains of half-wavelength dipoles at 0.25 mm from the planar layered models of the human body.

B. Optimal Antenna Sizes and Performances

Fig. 5 summarizes the maximum simulated gains G_{max} of dipoles and loops placed over the layered body models described in Tab. II for varying sides lengths L, while keeping fixed their thickness w to 160 μm and the distance from the body to 0.25 mm. Coherently with [31], there exists an optimal length L_{opt} at each of the considered frequencies where the gains are maximized. As in UHF, optimal loops exhibit a series resonance (the current is maximum at the input port) so that the expected bandwidth will be broader; moreover, they are three times smaller than the corresponding dipoles allowing to fit several antennas within the area of a medical-grade plaster.

Despite the higher body losses at both microwave and mmWave frequencies, the upper-bound gains and radiation efficiencies (η_r) are much higher than at UHF (Tab. III) because the outer skin acts as a reflector that reduces the amount of power delivered into the inner layers.

TABLE III: Size and Performances of Optimal Epidermal Antennas

Freq. (GHz)	L_{opt} (mm)	G_{opt} (dBi)	η_r (%)	Type
0.870 [31]	140	-12.6	0.3	Dip.
	45	-14.2	0.3	Loop
3.6	55	-4.6	6.5	Dip.
	17.5	-5.1	8	Loop
28	9	-1.7	9.7	Dip.
	3	-2.7	10.4	Loop
60	4.5	2.3	21.2	Dip.
	1.75	1.6	21.4	Loop

Fig. 6a compares the simulated upper-bound gains with the desired ones expressed through (5), for $a = G_T(f_{UHF})/f_{UHF}^2$, to evaluate the possibility of preserving, at 5G, the same range performance as in UHF. Up to 4 GHz, the degradation due to the path loss can be almost entirely compensated by the gain improvements of an epidermal antenna and, accordingly, similar UHF link ranges are expected with reduced antenna sizes. At higher frequencies, instead, there exists a drastic gap between the desired and the simulated gains. Hence, despite the relevant increase of the antenna gain at 28 GHz and 60 GHz, it is not pos-

2469-7281 (c) 2020 IEEE. Personal use is permitted, but republication/redistribution requires IEEE permission. See http://www.ieee.org/publications_standards/publications/rights/index.html for more information.
Authorized licensed use limited to: Universita degli Studi di Roma Tor Vergata. Downloaded on June 04,2020 at 11:13:04 UTC from IEEE Xplore. Restrictions apply.

This article has been accepted for publication in a future issue of this journal, but has not been fully edited. Content may change prior to final publication. Citation information: DOI 10.1109/JRFID.2020.2998082, IEEE Journal of Radio Frequency Identification

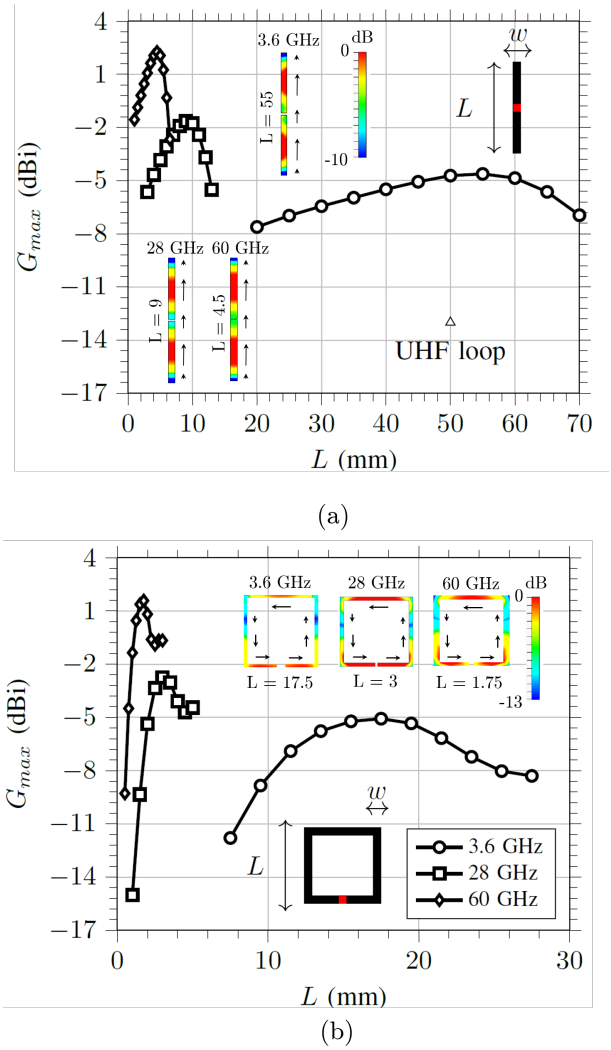

Fig. 5: Optimal gains of epidermal (a) dipoles and (b) loops as function of the length L. Distances of the radiating elements from the skin and antenna width are fixed at 0.25 mm and w = 160 μm, respectively. Insets: antenna dimensions and normalized surface currents for the optimal layouts.

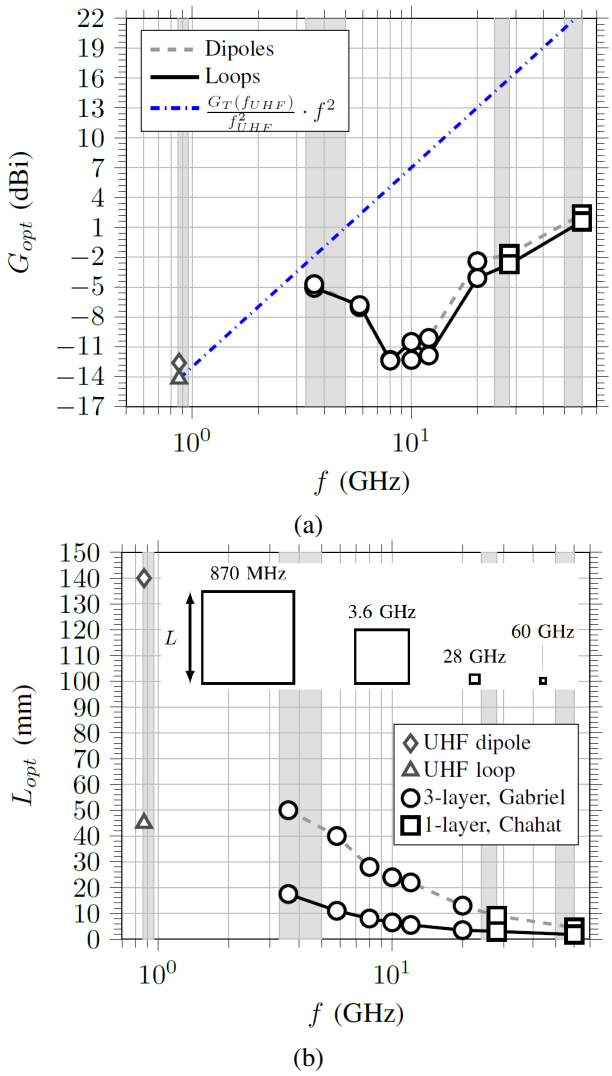

Fig. 6: (a) Upper-bound gains (dipoles and loops) at 5G frequencies compared with the theoretical quadratic law in (5) that would ensure a read range independent from the frequency; (b) optimal epidermal antenna sizes. Inset: in-scale view of epidermal loops. Data are compared with UHF loop and dipole [31]. The UHF and 5G frequencies bands of interest are highlighted in gray.

sible to achieve the same read range as in UHF with a single element and, as discussed in Sec. IV, arrays will be required. Finally, performances strongly degrade within the 7 - 20 GHz frequency range because of relaxation of the human body tissues, therefore, this frequency region must be avoided. Fig. 6b highlights the advantages of operating either at microwave or mmWave frequencies in terms of antenna footprints. At these frequencies, in fact, both the dipole and the loop side lengths L are significantly lowered. Microwave frequencies allow to reduce the footprint without requiring complex manufacturing processes while mmWave frequencies give a significant advantage for fitting several antennas within the area of a medical-grade plaster. Nonetheless, at these higher frequencies, more complex manufacturing methods will be required.

C. Experimental Corroboration

Simulations discussed so far have been verified at 3.6 GHz and at 28 GHz throughout experimentation on a roasted pork (estimated parameters ϵ_r = 40, σ = 2 S/m). Planar half-loops and monopoles (trace width w = 1 mm) of different lengths L were manufactured over a PET substrate (thickness t = 135 μm, ϵ_r = 3, $\tan\delta$ = 0.019) with adhesive copper that was carved out by a two-axis cutter. Antennas were mounted on a ground plane and vertically attached onto the phantom (Fig. 7a); gains were indirectly measured through a test monopole. The S_{21} scattering parameters were measured by a VNA (HP 8517A), upon calibration. Results of normalized $|S_{21}|^2$ (proportional to the normalized antenna gains G [34]) are plotted in Fig. 7b and compared with the corresponding simulations. Despite a small shift, due to the manufacturing imperfections and, above all, to the approximate resemblance

2469-7281 (c) 2020 IEEE. Personal use is permitted, but republication/redistribution requires IEEE permission. See http://www.ieee.org/publications_standards/publications/rights/index.html for more information.
Authorized licensed use limited to: Universita degli Studi di Roma Tor Vergata. Downloaded on June 04,2020 at 11:13:04 UTC from IEEE Xplore. Restrictions apply.

This article has been accepted for publication in a future issue of this journal, but has not been fully edited. Content may change prior to final publication. Citation information: DOI 10.1109/JRFID.2020.2998082, IEEE Journal of Radio Frequency Identification

between simulated and real phantoms, the presence of the numerically predicted optimal sizes are reasonably verified.

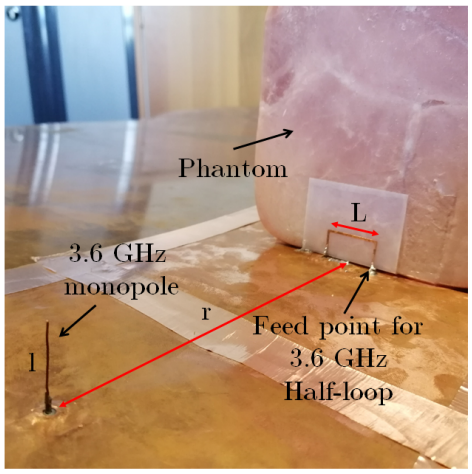

(a)

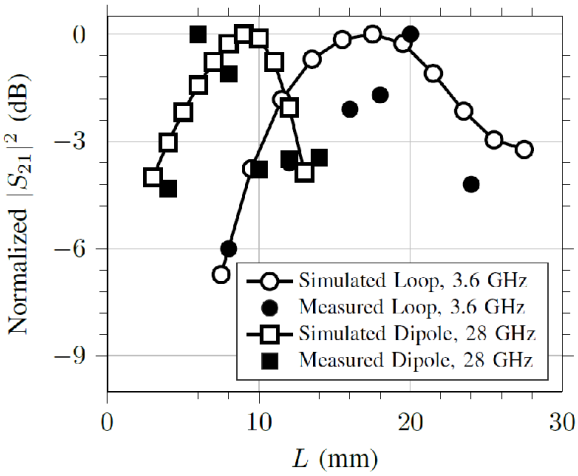

(b)

Fig. 7: (a) Experimental setup for measuring the gains of half-loops and monopoles when attached onto a roasted pork; probe monopole length l = {20, 2} mm and r = {13, 6} cm @ {3.6, 28} GHz, respectively. (b) Comparison between measured and simulated normalized gains as function of the size *L* of the epidermal antenna.

IV. Epidermal Arrays

When moving from UHF to mmWave, the effective antenna aperture can be preserved by replacing the single epidermal element with an array. Let r_{5G}^{max} denote the maximum activation distance of the transponder at the 5G frequency (f_{5G}) in a *b2b* link; by assuming that the transponder chip sensitivity at f_{5G} is equal to that at f_{UHF}, and that the same reader output power can be used, then, from (4):

$$\frac{r_{UHF}^{max}}{r_{5G}^{max}} = \sqrt{\frac{G_{T,UHF}}{G_{T,5G}(N)}} \frac{f_{5G}}{f_{UHF}}, \tag{6}$$

where $G_{T,5G}(N) \simeq NG_{T,5G}$ indicates the gain of an array of *N* epidermal 5G-RFID elements (with single-element gain $G_{T,5G}$). The minimum number N of required elements for the transponder array that would guarantee the same read distance as in UHF ($r_{5G}^{max} = r_{UHF}^{max}$) becomes:

$$N \geq \frac{G_{UHF}}{G_{5G}} \left(\frac{f_{5G}}{f_{UHF}} \right)^2. \tag{7}$$

By introducing in (7) the upper-bound gains G_{5G} of Tab. III, the resulting number of array elements can be found (Tab. IV). While the 3.6 GHz array could be feasible (a 2 x 2 array at most, with overall size of 6 cm x 6 cm), the 28 GHz and 60 GHz arrays would instead introduce a relevant and non-negligible complexity in the feeding network of an epidermal antenna, with a significant impact on size, cost and practical feasibility of the epidermal transponder.

TABLE IV: Number of Elements that Provide the Same Read Distance as in UHF

	3.6 GHz	28 GHz	60 GHz
Dipoles	3 (2x2)	85 (9x10)	154 (14x11)
Loops	3 (2x2)	74 (9x9)	126 (10x13)

A. Link Performance of a 5G-RFID Epidermal System

Examples of achievable read ranges are here given (Fig. 8) at the selected 5G frequencies (f_{5G}) and compared with a 30 x 30 mm^2 footprint which is the size of state-of-the-art UHF epidermal antennas [12]. The reference UHF *passive* chip sensitivity is $p_t = -15$ dBm and the corresponding theoretical maximum distance is r_{UHF}^{max} = 1.5 m for an Effective Isotropic Radiated Power (EIRP) of 4 W (36 dBm). The identified footprint is suitable to allocate either a single optimal loop at 3.6 GHz, or up to a 5 x 5 elements array (with an inter-element spacing shown in the inset of Fig. 8) at 28 GHz, or a 12 x 12 array at 60 GHz. At 60 GHz, fewer array elements are considered too. A summary of achievable ranges for different configurations and frequencies is reported in Fig. 8; the simulated achievable gains of both the single loop element and the full array models are given in Tab. V.

As shown in Fig. 8, a loop at 3.6 GHz allows a read distance of up to 1.3 m and a reduced size, while single element antennas at mmWave frequencies (*i.e.*: 28 GHz and 60 GHz) enable read distances of about 20 cm. From these results it emerges that the read distances at 3.6 GHz of both dipoles and loops are comparable with the ones achievable at UHF; moreover, 3.6 GHz loops have the added advantage of halving the antenna footprint (form 30 mm to 17.5 mm of side length). Even though much smaller than the UHF counterpart, the 28 GHz and 60 GHz single-element antennas could be used as modern high-speed NFC systems read through a 5G smartphone. Broadside loop arrays with *N* = 25 (@ 28 GHz) and N = 42 (@ 60 GHz) would return a maximum gain of 10.7 dBi and 17 dBi, respectively, guaranteeing ranges up to one meter. Finally, the N = 144 loop array at 60 GHz, that can be packed within the footprint of a single UHF loop, would enable a longer read range than in UHF (about 1.8 m).

B. Beam Steering

Multi-element epidermal loop arrays are suitable to beam-forming as in the 5 x 5 array example at 28 GHz of Fig. 9.

2469-7281 (c) 2020 IEEE. Personal use is permitted, but republication/redistribution requires IEEE permission. See http://www.ieee.org/publications_standards/publications/rights/index.html for more information.
Authorized licensed use limited to: Universita degli Studi di Roma Tor Vergata. Downloaded on June 04,2020 at 11:13:04 UTC from IEEE Xplore. Restrictions apply.

This article has been accepted for publication in a future issue of this journal, but has not been fully edited. Content may change prior to final publication. Citation information: DOI 10.1109/JRFID.2020.2998082, IEEE Journal of Radio Frequency Identification

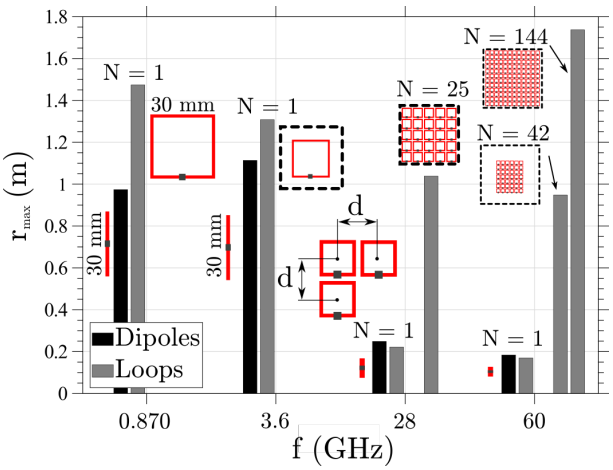

Fig. 8: Maximum link ranges of several dipole and loop tag configurations (all constrained within a 30 x 30 mm^2 footprint) at UHF and 5G frequencies for chip sensitivity p_t = -15 dBm. EIRP fixed to 4 W (36 dBm): P_{in} = 30 dBm and G_R = 6 dBi (*b2b* mode). Inter-element spacing for arrays: $d = \frac{\lambda_0}{2}$ = 5.36 mm at 28 GHz, and $d = \frac{\lambda_0}{2}$ = 2.5 mm at 60 GHz.

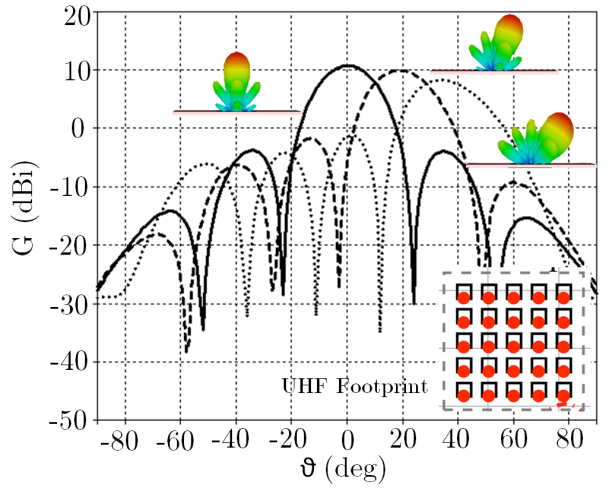

Fig. 9: Beamforming of the 28 GHz 5 x 5 loop array with inter-elements spacing $d = \lambda_0/2$ = 5.36 mm fitting within the 30 x 30 mm^2 footprint. Linear phase shifts: 63.3° for main lobe at 20° and 110° for main lobe at 40°.

The beam can be steered of 20° and 40° from the broadside without sensibly affecting the peak gain.

C. Data Rates

The higher gains provided by array configurations and the corresponding higher available bandwidths at 5G will enable relevant data-rates for *passive* 5G-RFIDs. By assuming a BPSK modulation, both the tag data-rate $R = 2B$ (with B being the RF bandwidth), and the Signal-to-Noise Ratio (SNR) are related by the equation [35]:

$$SNR|_{dB} = P_{R \leftarrow T}|_{dB} - BT_0k_B|_{dB} - NF|_{dB}, \quad (8)$$

with T_0 = 290 K being the system temperature, and $k_B = 1.3810^{-23}$ $\frac{m^2kg}{s^2K}$ the Boltzmann constant. By imposing a minimum SNR of 10 dB, an EIRP of 36 dBm, a reader antenna gain G_R = 6 dBi, a modulation index M = -6 dB, and a receiver noise figure NF = 10 dB, the maximum tag data-rate R can be computed from (8) for a single epidermal loop or for an array of loops placed one meter away from the reader (Tab. V). The highest date-rate occurs for the 3.6 GHz link (theoretically 0.52 Gbps). The evaluated data-rates are however intended as upper-bounds as the real achievable speed will depend on the specific frequency and bandwidth allocation of the 5G spectrum.

TABLE V: BPSK Data Rates of Passive 5G-RFID Links at 1 meter

Freq. (GHz)	Elements N	Gain (dBi)	Tag Rate (Gbps)
3.6	1 loop	-5.1	0.52
28	5 x 5 loops	10.7	0.36
60	12 x 12 loops	17	0.31

V. Electromagnetic Exposure

The results shown above revealed that the backscattering links enabled by future passive 5G-RFID epidermal sensors require the readers to be at a distance of 1-1.5 m from the human body at 3.6 GHz and at 17 cm at 60 GHz. Therefore, it is necessary to investigate the human exposure to high-frequency electromagnetic fields radiated by a nearby source to assess the safe implementation and the social acceptance of epidermal sensor networks.

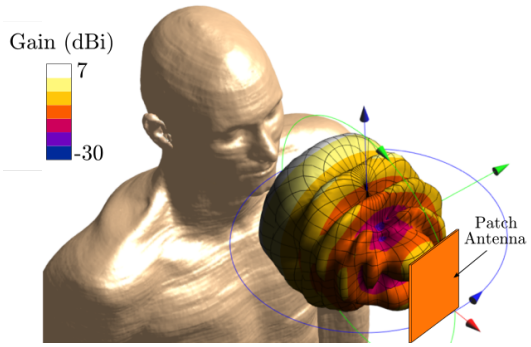

Fig. 10: Radiation pattern at 3.6 GHz of a 30 x 36 mm^2 patch antenna placed in front of the human head.

Fields induced into the human body by a nearby source at the lower 5G frequency (3.6 GHz) are numerically evaluated through the Specific Absorption Rate ($SAR = \frac{P_{diss}}{m}$, with P_{diss} being the electric power absorbed in tissue and m the tissue mass). For computing the SAR levels, the following simulation has been held with *Sim4Life 5.0*©: a patch reader antenna radiating an EIRP of 36 dBm is placed at distances h of 20 cm and 5 cm, respectively (Fig. 10), from the head (at eye level) of a high-resolution anatomical model of a 34-year-old man [36]. Peak spatial average SAR in 1g of tissue has been determined according to IEEE 62704-1-2017 - IEC/IEEE International Standard and, as shown in Fig. 11, peaks are localized around the eyes. For h = 20 cm, values are well below 0.5 $\frac{W}{kg}$ with a peak in correspondence of the aqueous humor and a sharp attenuation in the first 10 mm of tissue. By moving the radiating antenna closer to the face

2469-7281 (c) 2020 IEEE. Personal use is permitted, but republication/redistribution requires IEEE permission. See http://www.ieee.org/publications_standards/publications/rights/index.html for more information.
Authorized licensed use limited to: Universita degli Studi di Roma Tor Vergata. Downloaded on June 04,2020 at 11:13:04 UTC from IEEE Xplore. Restrictions apply.

This article has been accepted for publication in a future issue of this journal, but has not been fully edited. Content may change prior to final publication. Citation information: DOI 10.1109/JRFID.2020.2998082, IEEE Journal of Radio Frequency Identification

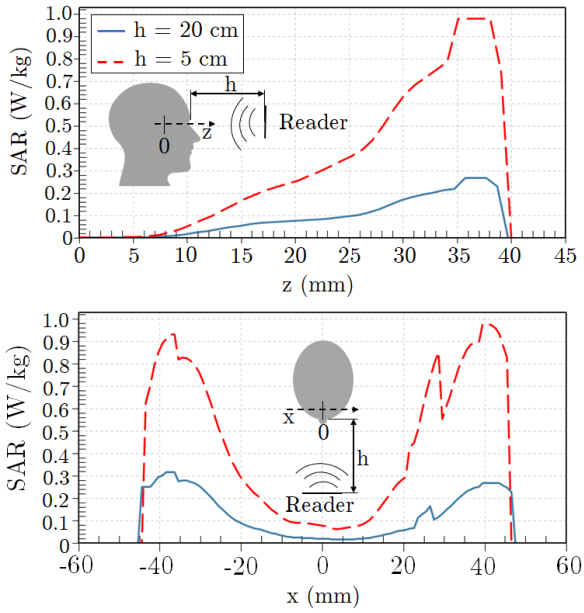

Fig. 11: SAR distributions in the head for a source emitting an EIRP of 36 dBm placed respectively 5 and 20 cm away from the face, at eyes level. FCC limit: SAR $< 1.6\ \frac{W}{kg}$ averaged over 1g of tissue [18].

(h = 5 cm), values increase up to 1 $\frac{W}{kg}$ around the eyes. However, in either cases, SAR values are compliant with the FCC conservative restriction of 1.6 $\frac{W}{kg}$ averaged over 1g of tissue and the absorption of power is confined within the first millimeters of the skin.

At 28 GHz and 60 GHz, instead, electromagnetic compliance is investigated through the power density $PD = \frac{EIRP}{4\pi h^2}$ emitted, in free space, by the reader located at distance h from the body. ICNIRP and FCC guidelines require $PD < 10\ \frac{W}{m^2}$ for the general public and $PD < 50\ \frac{W}{m^2}$ for the occupational group [18]. Even at the shortest ranges the power densities for EIRP = 36 dBm are below both the occupational groups and the general public restrictions (Fig. 12). For the sake of safety, the radiating source should be kept at 20 cm far from the body.

VI. Summary of the Results and Conclusions

This work allowed to achieve the following results:

i) backscattering communication links would be feasible in the 5G context. Despite the high losses of the human body, epidermal antennas operating at microwave and mmWave frequencies provide higher gains and higher radiation efficiencies (η_r) than those at UHF;

ii) at microwaves (3.6 GHz), an epidermal sensor with a single antenna element can achieve similar performances of UHF tags, even with a size smaller than 30 x 30 mm^2 (Tab. VI);

iii) at higher frequencies, single radiators could be adopted for short-range links with high data-rates that would improve NFC systems currently used in smartphones and wearable devices;

iv) array configurations are needed for links operating above 6 GHz to both establish longer communication ranges (in $b2p$ and $p2p$ links) and for implementing beamsteering operations;

v) both microwave and mmWave links allow higher data rates than at UHF for real-time transfer of data;

vi) passive 5G-RFID epidermal systems are compliant with electromagnetic exposure regulations for a reader-to-body distance longer than 5 cm (at 3.6 GHz) and 20 cm (at 28 GHz and 60 GHz), but arrays should be preferred for this second case;

vii) by comparing the electromagnetic performances of the optimal 5G loop at 3.6 GHz with the state-of-the-art UHF passive epidermal RFIDs, and by assuming the chip sensitivity p_t of -15 dBm, it is clear (Tab. VI) that the 3.6 GHz band looks particularly attractive since the epidermal antenna exhibits a higher aperture efficiency (η_A), a smaller size, and a comparable read range. However, a deeper experimental effort is still needed to exploit the above results in real configurations and it will be the topic of future research.

TABLE VI: State-of-the-art of Epidermal Antennas

Antenna type	Band	Size (mm^2)	Gain (dBi)	η_A (%)	r_{max} (m)
5G loop	3.6 GHz	17.5x17.5	≤-5.1	55.8	1.3
Thin wire [12]	UHF	30x30	≤-17.5	49.2*	1.3
Integrated tag [8]	UHF	30x30	≤-15	31.1*	1.7
Tattoo tag [11]	UHF	20x65	≤-16.5	15.2*	1.4

*Ref. frequency: 900 MHz

Although the results shown in this work suggest an upper bound communication range for passive epidermal 5G-RFIDs, it is important to stress out that ranges can be further improved if the same solutions currently explored at microwave frequencies (e.g.: Van Atta arrays [37] and Tunneling Tags [38]) are adopted and semi-passive solutions are taken into account. Epidermal 5G-RFIDs, by operating at frequency bands higher than UHF, can enable applications such as tracking with

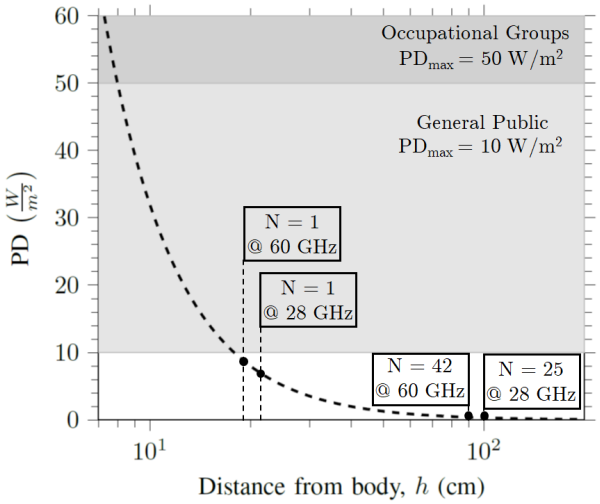

Fig. 12: Power density *vs* distance from the reader. EIRP fixed to 4 W (36 dBm). Values of the maximum link ranges shown in Fig. 8 are here compared with the FCC and ICNIRP restrictions for General Public $PD_{max} = 10\ \frac{W}{m^2}$ and occupational group $PD_{max} = 50\ \frac{W}{m^2}$.

2469-7281 (c) 2020 IEEE. Personal use is permitted, but republication/redistribution requires IEEE permission. See http://www.ieee.org/publications_standards/publications/rights/index.html for more information.
Authorized licensed use limited to: Universita degli Studi di Roma Tor Vergata. Downloaded on June 04,2020 at 11:13:04 UTC from IEEE Xplore. Restrictions apply.

This article has been accepted for publication in a future issue of this journal, but has not been fully edited. Content may change prior to final publication. Citation information: DOI 10.1109/JRFID.2020.2998082, IEEE Journal of Radio Frequency Identification

mm- and micro-scale resolutions [39] for medical applications (*e.g.*: micro-ablation or muscular and neural rehabilitation). Overall, 5G-RFIDs will be easily integrated within the automotive industry where mmWave radars are already being widely deployed [40] thus stimulating new types of driver-car interactions. Finally, the integration of RFID readers within future 5G mobile devices will reduce manufacturing costs and make RFIDs available to several new users.

REFERENCES

[1] D. H. Kim, N. Lu, R. Ma *et al.*, "Epidermal electronics," *Science*, vol. 333, no. 6044, pp. 838–843, Aug. 2011.

[2] H. U. Chung, B. H. Kim, J. Y. Lee *et al.*, "Binodal, wireless epidermal electronic systems with in-sensor analytics for neonatal intensive care," *Science*, vol. 363, no. 6430, 2019.

[3] A. Vaz, A. Ubarretxena, I. Zalbide *et al.*, "Full passive UHF tag with a temperature sensor suitable for human body temperature monitoring," *IEEE Transactions on Circuits and Systems II: Express Briefs*, vol. 57, no. 2, pp. 95–99, 2010.

[4] M. C. Caccami, M. Y. S. Mulla, C. Occhiuzzi, C. Di Natale, and G. Marrocco, "Design and experimentation of a batteryless on-skin RFID graphene-oxide sensor for the monitoring and discrimination of breath anomalies," *IEEE Sensors Journal*, vol. 18, no. 21, pp. 8893–8901, 2018.

[5] C. Miozzi, S. Nappi, S. Amendola, C. Occhiuzzi, and G. Marrocco, "A general-purpose configurable RFID epidermal board with a two-way discrete impedance tuning," *IEEE Antennas and Wireless Propagation Letters*, vol. 18, no. 4, pp. 684–687, April 2019.

[6] S. Nappi, V. Mazzaracchio, L. Fiore, F. Arduini, and G. Marrocco, "Flexible pH sensor for wireless monitoring of the human skin from the medimun distances," in *2019 IEEE International Conference on Flexible and Printable Sensors and Systems (FLEPS)*, 2019, pp. 1–3.

[7] F. Arduini, S. Cinti, V. Scognamiglio, D. Moscone, and G. Palleschi, "How cutting-edge technologies impact the design of electrochemical (bio)sensors for environmental analysis. A review," *Analytica Chimica Acta*, vol. 959, pp. 15 – 42, 2017. [Online]. Available: http://www.sciencedirect.com/science/article/pii/S0003267016315100

[8] C. Miozzi, S. Nappi, S. Amendola, C. Occhiuzzi, and G. Marrocco, "A general-purpose configurable RFID epidermal board with a two-way discrete impedance tuning," *IEEE Antennas and Wireless Propagation Letters*, vol. 18, no. 4, pp. 684–687, April 2019.

[9] R. B. V. B. Simorangkir, Y. Yang, R. M. Hashmi *et al.*, "Polydimethylsiloxane-embedded conductive fabric: Characterization and application for realization of robust passive and active flexible wearable antennas," *IEEE Access*, vol. 6, pp. 48 102–48 112, 2018.

[10] C. Miozzi, S. Amendola, A. Bergamini, and G. Marrocco, "Reliability of a re-usable wireless epidermal temperature sensor in real conditions," in *2017 IEEE 14th International Conference on Wearable and Implantable Body Sensor Networks (BSN)*, May 2017, pp. 95–98.

[11] M. A. Ziai and J. C. Batchelor, "Temporary on-skin passive UHF RFID transfer tag," *IEEE Transactions on Antennas and Propagation*, vol. 59, no. 10, pp. 3565–3571, Oct 2011.

[12] F. Amato, C. Miozzi, S. Nappi, and G. Marrocco, "Self-tuning UHF epidermal antennas," in *2019 IEEE 10th International Conference on RFID - Technology and Applicaitons (RFID-TA)*, Sept 2019, p. in press.

[13] S. Amendola, V. Di Cecco, and G. Marrocco, "Numerical and experimental characterization of wrist-fingers communication link for RFID-based finger augmented devices," *IEEE Transactions on Antennas and Propagation*, vol. 67, no. 1, pp. 531–540, Jan 2019.

[14] J. G. Andrews, S. Buzzi, W. Choi *et al.*, "What will 5G be?" *IEEE Journal on Selected Areas in Communications*, vol. 32, no. 6, pp. 1065–1082, June 2014.

[15] N. F. M. Aun, P. J. Soh, A. A. Al-Hadi *et al.*, "Revolutionizing wearables for 5G: 5G technologies: Recent developments and future perspectives for wearable devices and antennas," *IEEE Microwave Magazine*, vol. 18, no. 3, pp. 108–124, May 2017.

[16] A. Pellegrini, A. Brizzi, L. Zhang *et al.*, "Antennas and propagation for body-centric wireless communications at millimeter-wave frequencies: A review [wireless corner]," *IEEE Antennas and Propagation Magazine*, vol. 55, no. 4, pp. 262–287, Aug 2013.

[17] T. Tuovinen, M. Berg, A. Pärssinen, and E. Salonen, "Potential of a small array at 10 GHz for switchable on/off-body wearable sensor node purposes," in *2015 Loughborough Antennas Propagation Conference (LAPC)*, Nov 2015, pp. 1–5.

[18] T. Wu, T. S. Rappaport, and C. M. Collins, "Safe for generations to come: Considerations of safety for millimeter waves in wireless communications," *IEEE Microwave Magazine*, vol. 16, no. 2, pp. 65–84, March 2015.

[19] P. Pursula, T. Vaha-Heikkila, A. Muller *et al.*, "Millimeter-wave identification—a new short-range radio system for low-power high data-rate applications," *IEEE Transactions on Microwave Theory and Techniques*, vol. 56, no. 10, pp. 2221–2228, Oct 2008.

[20] F. Amato, S. Amendola, and G. Marrocco, "Upper-bound performances of RFID epidermal sensor networks at 5G frequencies," in *2019 IEEE 16th International Conference on Wearable and Implantable Body Sensor Networks (BSN)*, May 2019, pp. 1–4.

[21] 3GPP, "Study on Scenarios and Requirements for Next Generation Access Technologies (Release 14)," 3GPP, Tech. Rep., 08 2017.

[22] European Commission, "European commission to harmonise the last pioneer frequency band needed for 5G deployment," (Accessed May. 7, 2020). [Online]. Available: ec.europa.eu/digital-single-market/en/news/european-commission-harmonise-last-pioneer-frequency-band-needed-5g-deploymentl

[23] Huawei, "5G Spectrum Public Policy Position," Huawei, Tech. Rep., 2018.

[24] O. Galinina, K. Mikhaylov, K. Huang, S. Andreev, and Y. Koucheryavy, "Wirelessly powered urban crowd sensing over wearables: Trading energy for data," *IEEE Wireless Communications*, vol. 25, no. 2, pp. 140–149, April 2018.

[25] H. T. Friis, "A note on a simple transmission formula," *Proceedings of the IRE*, vol. 34, no. 5, pp. 254–256, May 1946.

[26] G. Marrocco, "The art of UHF RFID antenna design: impedance-matching and size-reduction techniques," *IEEE Antennas and Propagation Magazine*, vol. 50, no. 1, pp. 66–79, Feb 2008.

[27] Axzon, (Accessed May. 7, 2020).

[28] "Zebra FX7500," (Accessed May. 7, 2020). [Online]. Available: www.zebra.com/gb/en/products/spec-sheets/rfid/rfid-readers/fx7500.html

[29] "Zebra FX9600," (Accessed May. 7, 2020). [Online]. Available: www.zebra.com/gb/en/products/spec-sheets/rfid/rfid-readers/fx9600.html

[30] "Impinj Indy RS2000," (Accessed May. 7, 2020). [Online]. Available: support.impinj.com/hc/en-us/articles/204969718-Indy-RS2000-Datasheet

[31] S. Amendola and G. Marrocco, "Optimal performance of epidermal antennas for UHF radio frequency identification and sensing," *IEEE Transactions on Antennas and Propagation*, vol. 65, no. 2, pp. 473–481, Feb 2017.

[32] D. Andreuccetti, R. Fossi, and C. Petrucci, "Dielectric properties of body tissues," (Accessed May. 7, 2020). [Online]. Available: niremf.ifac.cnr.it/tissprop/htmlclie/htmlclie.php

[33] N. Chahat, M. Zhadobov, R. Augustine, and R. Sauleau, "Human skin permittivity models for millimetre-wave range," *Electronics Letters*, vol. 47, no. 7, pp. 427–428, March 2011.

[34] C. A. Balanis, *Antenna theory: analysis and design*. John Wiley & Sons, Inc, 2016.

[35] J. Proakis, *Digital Communications: 4th ed.* McGraw-Hill Companies, 2000.

[36] "Human phantom Duke - ITIS foundationi," (Accessed May. 7, 2020). [Online]. Available: itis.swiss/virtual-population/virtual-population/overview/

[37] M. Alhassoun, M. A. Varner, and G. D. Durgin, "Theory and design of a retrodirective rat-race-based RFID tag," *IEEE Journal of Radio Frequency Identification*, pp. 1–1, 2018.

[38] F. Amato, H. M. Torun, and G. D. Durgin, "RFID backscattering in long-range scenarios," *IEEE Transactions on Wireless Communications*, vol. 17, no. 4, pp. 2718–2725, April 2018.

[39] C. Qi, F. Amato, M. Alhassoun, and G. D. Durgin, "Breaking the range limit of RFID localization: Phase-based positioning with tunneling tags," in *2019 IEEE International Conference on RFID (RFID)*, 2019, pp. 1–8.

[40] G. Serafino, F. Amato, S. Maresca *et al.*, "Photonic approach for on-board and ground radars in automotive applications," *IET Radar, Sonar Navigation*, vol. 12, no. 10, pp. 1179–1186, 2018.

2469-7281 (c) 2020 IEEE. Personal use is permitted, but republication/redistribution requires IEEE permission. See http://www.ieee.org/publications_standards/publications/rights/index.html for more information.
Authorized licensed use limited to: Universita degli Studi di Roma Tor Vergata. Downloaded on June 04,2020 at 11:13:04 UTC from IEEE Xplore. Restrictions apply.

This article has been accepted for publication in a future issue of this journal, but has not been fully edited. Content may change prior to final publication. Citation information: DOI 10.1109/JRFID.2020.2998082, IEEE Journal of Radio Frequency Identification

Francesco Amato received his B.S. and M.S. in Telecommunication Engineering from the University of Roma Tor Vergata in 2006 and 2009, respectively and the Ph.D degree in Electrical and Computer Engineering from the Georgia Institute of Technology, Atlanta, GA (USA) in January 2017. In 2017 and 2018 he was a postdoctoral researcher at the Sant'Anna School of Advanced Studies (Pisa); he is currently a postodoctoral researcher at the University of Roma Tor Vergata. From 2009 to 2011 he worked at SES (Luxembourg) as Ground System Engineer. In 2012 he joined the Propagation Group at the Georgia Institute of Technology as Fulbright Research Scholar and was a Research Intern at Intel Labs, Santa Clara, CA (USA) in 2015. His research interests include wireless radio communications, microwave circuits and mmWave antenna design. He was a *Fulbright* Scholar (2012 - 2016) and a GoSTEM Fellow (2013 and 2014). In 2015, he was awarded the *William Brown* Fellowship and the Best Student Paper Award at the IEEE International Conference on RFID-Technologies and Applications (RFID-TA), Tokyo (Japan). In 2019, he was the recipient of both the Best Paper Award at the IEEE International Conference on RFID, Phoenix (AZ, USA), and the *Clive Hohberger* Technology Award at the RFID Journal Live! He was organizing committee member for the IEEE International Conference on RFID (2017 - 2020) and the IEEE RFID-TA in 2019.

Cecilia Occhiuzzi received the M.Sc. degree in medical engineering and Ph.D. degree in electromagnetics from the University of Roma Tor Vergata, Rome, Italy, in 2008 and 2011, respectively. Currently, she is Assistant Professor with the University of Roma Tor Vergata, where she teaches Electromagnetic Fields. In 2008, she was with the School of Engineering, University of Warwick, Coventry, U.K. as a post-graduate student, in 2010, she was a Visiting Researcher with the Georgia Institute of Technology, Atlanta, GA, USA and in 2014 she was a Research Assistant with the University of Palermo, Italy. She is the Co-Founder and CEO of RADIO6ENSE. Her research interests include wireless health monitoring by means of wearable and implantable radio-frequency/mm-wave identification techniques and pervasive sensing paradigms for Industry 4.0. Dr. Occhiuzzi was the recipient of the IEEE APS Doctoral Award, in 2011. In 2012, she was the recipient of the Best Thesis Award at the 2012 RFID Journal Live, Orlando, FL, USA. She is author of more than sixty papers on International Journals and Conferences.

Gaetano Marrocco received the Laurea in Electronic Engineering and Ph.D. in Applied Electromagnetics at the University of L'Aquila, Italy, in 1994 and 1998, respectively. He has been researcher at the University of Roma Tor Vergata in 1994-2014 and Associate Professor of Electromagnetics in 2013-2017; Guest Professor at the University of Paris-est Marne la Vallèe in 2015 and Full Professor at the University of Roma Tor Vergata since 2018. He currently serves as Director of the Medical Engineering School. His research is mainly directed to the modelling and design of broadband and ultra-wideband (UWB) antennas and arrays as well as of sensor-oriented miniaturized antennas for Biomedical Engineering, Aeronautics and Radiofrequency Identification (RFID). During the last decade, he carried out pioneering research on the wireless-activated sensors, and in particular on Wearable and Epidermal Electronics, contributing to move from the labeling of objects to the passive sensor networks in the Internet of Things era. He serves as Associate Editor of the IEEE Journal of Radiofrequency Identification and was member of the IEEE Antennas and Propagation Society Awards committee. He is moreover Chair of the Italian delegation URSI Commission D Electronics and Photonics. He was the chair of the Local Committee of the V European Conference on Antennas and Propagation (EUCAP-2011), TPC chair of the 2012 IEEE-RFID TA in Nice, France, TPC track-chair of the 2016 IEEE Antennas and Propagation Int. Symposium, TPC track-chair of IEEE-RFID 2018 USA. Prof. Marrocco is the director of the Pervasive Electromagnetics Lab and the co-founder and president of the University spin-off RADIO6ENSE (www.radio6ense.com) active in the short-range electromagnetic sensing for Industrial Internet of Things, Smart Manufacturing, Automotive and Physical Security.

2469-7281 (c) 2020 IEEE. Personal use is permitted, but republication/redistribution requires IEEE permission. See http://www.ieee.org/publications_standards/publications/rights/index.html for more information.
Authorized licensed use limited to: Universita degli Studi di Roma Tor Vergata. Downloaded on June 04,2020 at 11:13:04 UTC from IEEE Xplore. Restrictions apply.